Journal of Materials Chemistry A

Accepted Manuscript

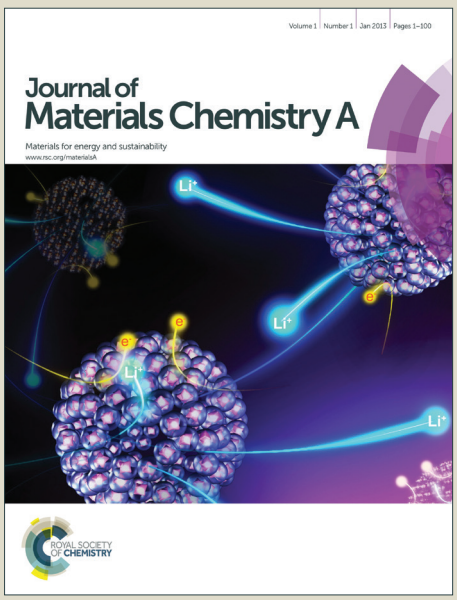

ROYAL SOCIETY OF CHEMISTRY

www.rsc.org/materialsA

Cite this: DOI: 10.1039/c0xx00000x

www.rsc.org/xxxxxx

ARTICLE TYPE

Porous magnetic carbon sheets from biomass as super adsorbent for fast removal of organic pollutants from aqueous solution

Shouwei Zhang,[a,b] Meiyi Zeng,[b] Jiaxing Li,[*a] Jie Li,[a] Jinzhang Xu[b] and Xiangke Wang[*a,c]

Received (in XXX, XXX) Xth XXXXXXXXX 20XX, Accepted Xth XXXXXXXXX 20XX

DOI: 10.1039/b000000x

A facile and scalable *in-situ* synthetic strategy (simultaneous template-graphitization) was developed to fabricate carbon-stabilized Fe/Fe_3C nanoparticles, which were homogeneously embedded in porous carbon sheets (PMCS) as excellent adsorbent for wastewater treatment. For the synthesis, the graphitic catalyst precursor ($Fe(NO_3)_3$) and template agent ($Al(NO_3)_3$) were introduced simultaneously into the agar hydrogel through the coordination of the metal precursor with the functional groups of agar, thus making simultaneous realization of template and graphitization of the carbon source under heat treatment. PMCS with high surface area (1023.2 m^2/g) exhibited high adsorption capacities and fast adsorption rates toward dyes. By using methylene blue (MB), methyl orange (MO) and crystal violet (CV) as model pollutants, the maximum adsorption capabilities for MB, MO, and CV reached up to 1615.9, 1062.4 and 1728.3 mg/g, respectively. Moreover, the magnetic separation also facilitated its application in wastewater treatment in large scale. This multifunctional material can be potentially used as super absorbents to remove pollutants efficiently from the wastewater.

1 Introduction

Recently, considerable amount of color wastewater has been generated from many industries, including textile, printing, paper, dyestuff, plastic and other industries, which is rather difficult to be treated because of their non-degradable synthetic origins and aromatic structures.[1] Meanwhile, water quality is highly influenced by dyes because they are highly visible and undesirable and most of them are considered to be toxic and even carcinogenic.[2, 3]

For the sake of human health and ecological security, it is very urgent to develop new approaches to removal dye from wastewaters, and those approaches should be inexpensive, swift, effective and environmental friendly. Among various removal processes, adsorption technology is more and more significant in field of fundamental studies and industrial applications for the easy operation and wide availability of adsorption materials.[4] In recent years, many kinds of carbon materials have been prepared and used for the removal of dyes and heavy metals due to their low cost, acid and alkali corrosion resistance, high specific surface area and enhanced adsorption capacity.[5] However, the applications of those carbon materials have some inherent limitations, such as the separation these carbon materials from the treated solution, especially for the nano-sized materials.[6] The conventional approach generally involves filtration or centrifugation, which is tedious, laborious, energy intensive and expensive, thus limiting their application in bulk wastewater treatment. Therefore, it is very intriguing to develop innovative adsorbent that can be easily and quickly removed from aqueous system.

The magnetically functionalized carbon materials have attracted extensive interests due to their easy separation.[7-14] Such carbon materials include γ-Fe_2O_3/CMK-3,[15] magnetic graphene nanocomposites,[16] multiwalled carbon nanotubes/iron oxides,[17] mesoporous magnetic iron oxide@carbon encapsulates,[18] and so on. However, most of those reported magnetic carbon materials are not very fit to be industrialized for the relatively poor stability and high cost. In particular, the magnetic substances can be corroded and leached by chemicals because they are open to the water. Moreover, the costs of some carbon materials, such as carbon nanotube or graphene, are extremely high due to their complex production processes.

From the viewpoint of economic, environmental and societal issues, porous carbon materials derived from renewable materials would be considered to be even more worthwhile due to their low cost and high practicability.[19, 20] However, until now there are few reports about the preparation of magnetic carbon materials using biomass or biomass derivatives for water treatment.[21] As a natural macromolecule multi-sugar product, agar extracted from porphyra and gracilaria seaweeds is cheap, renewable, environmental friendly and commercially available. However, it has not attracted any attention until now that agar is used as a promising precursor for porous magnetic carbon materials

Herein, we developed a facile and scalable *in-situ* synthetic strategy to fabricate carbon-stabilized magnetic (Fe/Fe_3C) nanoparticles homogeneously embedded in porous carbon sheets (designated as PMCS) with ultrahigh adsorption performance, fast separation from solution and excellent recyclable stability. Agar was used as the carbon sources due to its non-toxicity, low cost, natural abundance, environmental friendliness, and the most

important reason: the abundant -OH groups in agar have strong complexation with Fe/Al ions, lead to fix them in hydrogel matrix, and then avoid the aggregation of Fe/Fe_3C nanoparticles. So the Fe/Fe_3C nanoparticles can be homogeneously embedded in carbon nanosheets of PMCS. The prepared PMCS was fully characterized and its adsorption property including the effect of various parameters was fully investigated using MB, MO and CV as model pollutants. The possible adsorption mechanisms were also discussed.

2 Materials and methods

All reagents were of analytical grade and were commercially available from Sinopharm Chemical Reagent Co., Ltd (China) and were used without further purification.

Materials Preparation

PMCS was synthesized through a facile simultaneous template-graphitization route by using $Fe(NO_3)_3{\cdot}9H_2O$, $Al(NO_3)_3{\cdot}9H_2O$ and agar as the graphitic catalyst, template agent and carbon source, respectively. For a typical procedure, 2 g agar was dissolved in 50 mL deionized water at 80 ^oC with continuous stirring for 3 h until the agar is fully dissolved. Solution containing 1 g $Fe(NO_3)_3{\cdot}9H_2O$ and 4 g of $Al(NO_3)_3{\cdot}9H_2O$ was added into the agar hydrosol and stirred for 24 h at 80 ^oC to reach a uniform mixture, and then dried in an oven at 80 ^oC. The obtained solid were grounded by agatemortar to obtain very fine powders and subsequently calcined in N_2 atmosphere at 800 ^oC for 1 h. The resultant black powders were immersed in dilute NaOH solution to remove Al_2O_3 template, and subsequently washed with excess deionized water, then dried under vacuum at 60 ^oC for 10 h to obtain the PMCS sample. Activated carbon (AC) from agar under same condition without $Fe(NO_3)_3{\cdot}9H_2O$ and $Al(NO_3)_3{\cdot}9H_2O$ was also synthesized.

Characterization

XRD patterns were recorded in reflection mode (Cu Kα radiation, λ = 1.5418 Å) using a Scintag XDS-2000 diffractometer. X-ray photoelectron spectroscopy (XPS) data were obtained with an ESCA Lab220i-XL electron spectrometer from VG Scientific using 300W Al Kα radiation. The morphologies and microstructures were observed using a field emission scanning electron microscope (FE-SEM, Sirion200, FEI Corp., Holland) and transmission electron microscopy (TEM, JEM-2011, JEOL, Japan). The UV-Vis spectra were recorded on a Shimadzu UV-2550 spectrophotometer equipped with a Labsphere diffuse reflectance accessory. Thermogravimetric analysis was performed with a NETZSCH TG209 F3 instrument under air at the heating rate of 20 ^oC/min. The Brunauer-Emmett-Teller (BET) method was used to calculate the specific surface areas. The N_2 adsorption-desorption isotherms at 77 K were measured using an adsorption instrument (TriStarII, Micromeritics Company, USA) to evaluate their pore structures. Raman spectra were recorded using a LabRamHR. The laser excitation was provided by a regular model laser operating at 514.5 nm. Fourier Transforms Infrared spectroscopy (FT-IR) was carried out on a Bruker EQUINOX55 spectrometer (Nexus) in KBr pellet at room temperature.

Adsorption Experiments

All adsorption experiments were carried out in glass vials (50 mL) by using batch technique. For the kinetic experiments, a stock suspension of 5 mg/mL (0.25 mL) PMCS was ultrasonically dispersed into 20 mL of 50 mg/L dye (MB, MO or CV) solution for 1 min, then shaken for 24 h. Samples were withdrawn at appropriate time intervals and supernatant was separated by centrifugation at 8500 rpm for 15 min. For the adsorption isotherm experiments, 0.25 mL of 5 mg/mL PMCS suspension was added to 20 mL of dye solution with various concentrations..The solid and liquid phases were separated by centrifugation at 8500 rpm for 15 min after the suspensions were oscillated for 24 h. The PMCS were recycled for eight times after achieving adsorption equilibrium with dyes each time. The doses of initial dye and PMCS were 150mg/L (20mL) and 5 mg/mL (0.25mL), respectively. The PMCS was separated from the aqueous phase by magnet each time, washed with 0.1 mol/L HNO_3 and deionized water several times, dried in vacuum at 60^oC, and weighed for the next reuse cycle. The concentrations of dye in supernatant were determined by UV-vis absorption spectroscopy, and the amounts of dye adsorbed on adsorbents were calculated by using the following equation:

$$q_e = \frac{(C_0 - C_e)V}{m}$$

where C_0 and C_e are the initial and equilibrium concentrations of dye (mg/L) respectively, V is the volume of solution (L) and m is the mass of PMCS used (g).

3 Results and discussion

Characterization of PMCS

The XRD pattern of PMCS was shown in Fig. 1A. The diffraction peak at 26.5° corresponded to the (002) planes of graphitic carbon, and the peaks at 44.8^o and 65.1^o indicated the presence of α-Fe (JCPDS, No. 87-0722). The rest of diffraction peaks were the characteristics of the crystalline planes of Fe_3C species (JCPDS, No. 89-2867).[22] From XRD results, it was confirmed that the composites consisted of graphite carbon and Fe/Fe_3C species. Figure 1B showed the Raman spectrum of PMCS. The diffraction peaks from 200 to 600 cm^{-1} was indexed to the phases of α-Fe and Fe_3C.[23] Therefore, both XRD and Raman results suggested that the species ofFe and Fe_3C was formed during the pyrolysis process. The content of Fe in the PMCS was evaluated by TGA analysis (Fig. 1C). At the end, the carbon became CO_2 gas and Fe/Fe_3C nanoparticles were oxidized into Fe_2O_3 after combustion in air. The result demonstrated that the contents of Fe_2O_3 were accordingly ~57.8 wt%. Thus the Fe content was calculated to be ~40.5 wt%. The nitrogen adsorption-desorption isotherm of PMCS was shown in Fig. 1D. The PMCS exhibited a small hysteresis loop in the relative pressure from 0.4 to0.9, demonstrating the microporosity and mesoporosity coexisted in the material.[20] The adsorption quantity increase dramatically at a relative pressure near to 1.0 due to the filling of space in PMCS. Based on the nitrogen quantity adsorbed at different relative pressures, the N_2-BET surface area of the PMCS was calculated to be 1023.2 m^2/g, total pore volume was 1.32 cm^3/g, and average pore diameter was 12.5 nm. There are great

deals of adsorption sites in the surface of PMCS due to its high surface area, which is beneficial for adsorption. Meanwhile, the porous structure is favorable for the rapid diffusion of dye by providing the interconnected and low-resistance channels for dye.

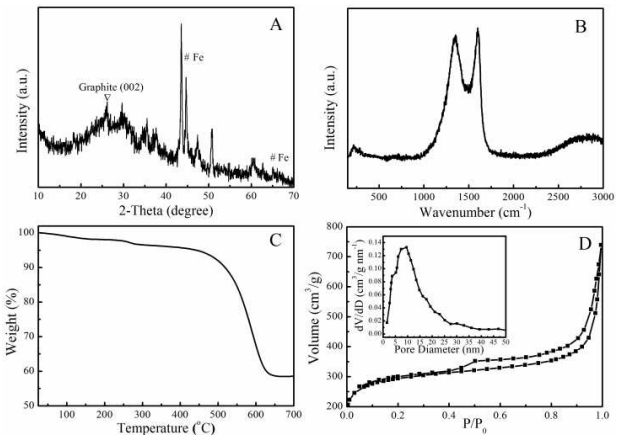

Fig. 1 The XRD pattern (A), Raman spectrum (B), TGA curve (C) and N_2 adsorption-desorption isotherm of PMCS.

The SEM image showed a very rough PMCS surface morphology (Fig. 2A), which was composed of large numbers of sheets-like and porous structures. The TEM image of PMCS was shown in Fig. 2B, one can see that the sample is mainly composed of stacked and folded few-layer and multilayer porous graphene-like sheets, which is beneficial to improve the adsorption of organic pollutants. The PMCS has a large sheet structure in planar and it therefore takes a short time for the dye molecules to transfer into and out of the inner porous network. That is, short diffusion channels can facilitate the permeation of the dyes between the PMCS, resulting in quick adsorption and ultrahigh adsorption capacity. This will be evidenced in the following section of dye sorption on PMCS.

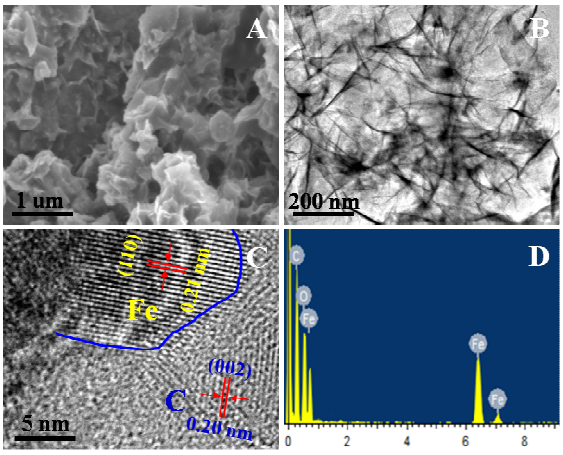

Fig. 2 The SEM (A), TEM (B) and HRTEM (C) image of the PMCS. (D) The EDS spectrum of the PMCS.

The detailed information of structure was further examined using HRTEM (Fig. 2C). The Fe/Fe_3C particle was surrounded by carbon. The lattice fringe with a distance of 2.1 Å, depicting a highly crystalline structure, corresponded to the (110) plane of α-Fe crystal. The outer lattice fringe with a calculated *d*-spacing of 2.0 Å corresponded to the (002) plane of graphite.[22] As the results from the energy-dispersive spectroscopy (EDS) analysis of the PMCS indicated in Fig. 2D, Fe, C and O were detected. Elemental mapping based on the PMCS indicated the distribution of three elements within the sheets structures (Fig. 3). It can be seen that the elements of Fe is homogeneously distributed in the carbon sheet, indicating that the Fe/Fe_3C is uniformly deposited on the carbon sheet surface.

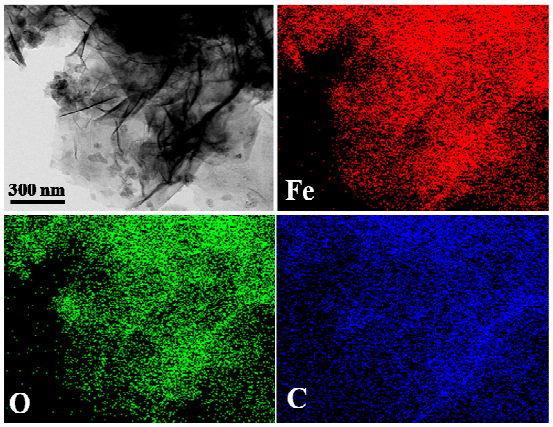

Fig. 3 The elemental mapping of the homogenous dispersion of Fe, O and C element in the PMCS.

High-resolution XPS spectra were performed to study the valence and electronic structure of Fe, O, and C in PMCS. The peaks of Fe, O, and C were observed in Fig. 4A. The C 1s peak was deconvoluted into four components Gaussian peaks (Fig. 4B). The main peak at 284.2 eV corresponded to the sp^2-hybridized graphite-like carbon atoms (C=C). Peak 2 centered at 285.1 eV was attributed to the sp^3-hybridized carbon atoms (C-C). Peaks at 287.8 eV and 289.9 eV were considered to C-O (e.g., alcohol, ether), and O-C=O (e.g., carboxylic, ester) species, respectively.[24] Fe 2p spectrum was composed of a doublet structure due to multiplets splitting (i.e., Fe $2p_{3/2}$ and Fe $2p_{1/2}$) as shown in Fig. 4C. The peaks at 706.4 eV and 708.5 eV were Fe^0 and Fe_3C, respectively.[25] With respect to the high resolution of O1s spectrum (Fig. 4D), three distinct peaks were identified: the peak located at 532.6 eV was due to C=O; the peak at 534.1 eV was derived from the contribution of C-OH/C-O-OH/N-O-C; and the peak at 535.8 eV corresponded to the physically adsorbed O_2/H_2O.[26]

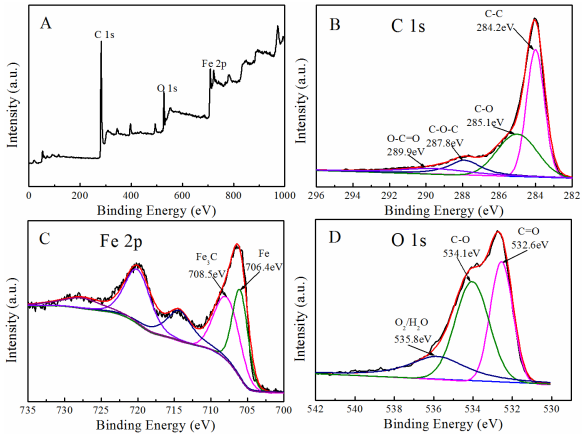

Fig. 4 The XPS analysis of PMCS: (A) survey spectrum; (B) C 1s spectrum; (C) Fe 2p spectrum; (D) O 1s spectrum.

Formation mechanism of PMCS

Generally, the graphene-like structure is formed by using a planar template.[27] In this study, PMCS was obtained by carbonizing the agar-Fe/Al composites and subsequently removing the Al. And no additional substrates were adopted during the synthesis processes. A rational formation processes were proposed, as illustrated in Fig. 5. The abundant -OH groups in agar had strong interaction with the Fe^{3+} and Al^{3+} ions, so some Fe^{3+}/Al^{3+} were adsorbed by the agar, formed agar-Fe/Al precursor.[28-30] Fe loaded on the biomass in the form of $Fe(NO_3)_3$ was hydrolyzed to Fe hydroxides (FeO(OH)) in the drying process.[20] Some Fe hydroxides (FeO(OH)) were formed due to the directly hydrolyzation of ferric iron.[31] These Fe hydroxides were wrapped by agar. At last, Fe species were uniformly dispersed in the agar matrix, and $Al(NO_3)_3$ had the similar process of transportation. The thermal decompositions of precursor at 800 ^oC for 1 h were totally different. In the case of $Fe(NO_3)_3{\cdot}9H_2O$, the iron salts was decomposed to Fe_3O_4 under mesothermal conditions at 400-600 ^oC. Fe_3C gradually formed and transformed into Fe subsequently (600-700 ^oC). Some carbon atoms were incorporated into iron oxide phase to form dense Fe_3C layers, then Fe_3C gradually formed and transformed into Fe subsequently (700 ^oC), which was important for the formation of the sheet-like carbon. When the carbonization temperatures further increased (800 ^oC), the active carbon atoms in Fe_3C layers could diffuse out to form dense 2D carbon-atom layers (sheets) on the surfaces of the formed planar "Fe-template" layers, and excess amount carbon atoms deposited on the formed sheets. The formed Fe_3C phase can act as a template to limit the carbon graphitization along with the 2D planar. In this forming process, the Fe catalyst was favorable to form a dense layer-like "Fe template" that limited the growth of the carbon atoms along the 2D planar. As for $Al(NO_3)_3{\cdot}9H_2O$, it decomposed into solid Al_2O_3, and gases such as nitrogen oxides, oxygen etc. at temperature above 400 ^oC. The produced Al_2O_3 substance was very stable at 800 ^oC and could not react with carbon from the carbonization of agar. Finally, PMCS was obtained after Al_2O_3 was further removed by sodium hydroxide solution. To sum up, Fe can form a carburized phase in the heating process, and the formation-decomposition process of the carburized phase can lead to the formation of graphene-like sheets. And Al_2O_3 obtained from the thermal decomposition of $Al(NO_3)_3{\cdot}9H_2O$ actually acted as hard templates for the formation of various pores in PMCS. Meanwhile, as another pore former, the associated gas gave a further improvement of the porosity during pyrolysis.

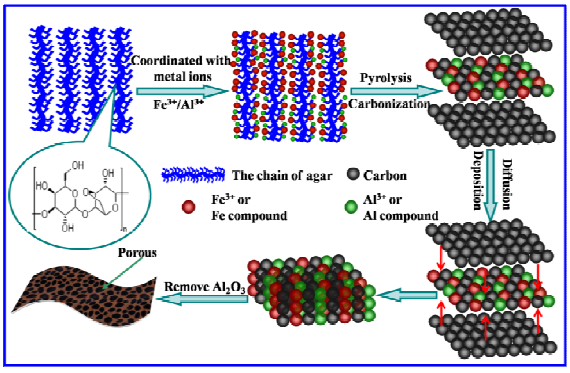

Fig. 5 The mechanism illustration of the decomposition of agar and formation of PMCS in the fast pyrolysis processes.

Ultrahigh adsorption capacity for dyes

The effect of contact time on the adsorption of MB, MO, and CV onto PMCS was investigated. As can be seen in Figs. 6A-6C, all adsorption curves kept the same trend, and only about 20% of pollutants were adsorbed onto active carbon (AC) within 60 min, implying AC possessed low adsorption capacity for those model pollutants. However, the removal curves of PMCS were found to be rapid and more than 99% of pollutants were removed at equilibrium within 40 min, suggesting PMCS possessed both high adsorption capacity and high removal rate for the removal of dyes from water.

To further understand the characteristics of the adsorption process, kinetic models such as pseudo-first-order and pseudo-second-order were exploited to analyze the experimental data (Supporting Information, SI). The calculated kinetics parameters for the removal of dye on PMCS were listed in Table S1.

Adsorption kinetics are usually controlled by different mechanisms, of which the most limiting ones are the diffusion mechanisms, including the initial curved portion, which is attributed to rapid external diffusion, and the linear portion, i.e. a gradual adsorption stage due to intraparticle diffusion.[32, 33] Consequently, the adsorption rate might be controlled by outer diffusion, inner diffusion or both. To further understand the adsorption process of MB, MO and CV, we applied the Weber-Morris equation:

$$q_t = K_d t^{1/2} + L$$

Piecewise linear regression of data showed that q_t *vs.* $t^{1/2}$ plots had two distinct regions, as shown in Figs. 6D-6F. The first linear portion included the adsorption period of 4-25 min, which represented external mass transfer. The second linear portion included the adsorption period of 25-100 min, representing intraparticle diffusion. That is, the first stage was external mass transfer resistance and the second was intra-particle mass transfer resistance. The two steps existed in the whole adsorption processes as follows: (1) the initial steep portion was a faster dye removal attributed to the adsorbate diffusion through solution to the adsorbent exterior surface (outer diffusion); (2) diffusion of adsorbate from the adsorbent exterior surface to the pores or capillaries of adsorbent internal structure (intraparticle diffusion).[34] It was also observed that the plots did not pass through the origin and large intercepts of the second linear portion of the plots, suggesting that the intraparticle diffusion was not the sole rate-controlling step and the external mass transfer also affected the adsorption rates.[35, 36] And for all the adsorptions of dyes, it took longer time for the process of intraparticle diffusion than the process of external mass transfer. Therefore, the overall adsorption process was controlled jointly by external mass transfer and intraparticle diffusion, and intraparticle diffusion was predominated over the external mass transfer.

Both Langmuir and Freundlich isotherms were used to describe the adsorption behavior of dyes on PMCS (SI). The equilibrium curves of MB, MO and CV on AC and PMCS were shown in Figs. 6G-6I. The corresponding adsorption isotherm constants of the two models were given in Table 1. For the adsorptions of MB,

MO and CV on AC and PMCS, both Langmuir and Freundlich models fitted the adsorption data well and gave similar correlation coefficients, which indicated that the dispersion of magnetic nanoparticles and distribution of adsorption sites on carbon sheets were uniform. The maximum capacities based on Langmuir model were 1615.9 mg/g for MB, 1062.4 mg/g for MO and 1728.3 mg/g for CV on PMCS, and 270.1 mg/g for MB, 209.5 mg/g for MO and 366.9 mg/g for CV on AC, respectively.

Table 1. The Langmuir and Freundlich isotherm model parameters of AC and PMCS.

		MB		MO		CV	
		PMCS	AC	PMCS	AC	PMCS	AC
Langmuir	q_m	1615.9	270.1	1062.4	209.5	1728.3	366.9
	b	0.2063	0.0614	0.1054	0.0136	0.0769	0.0105
	R^2	0.9861	0.9246	0.9638	0.9585	0.9924	0.8878
Freundlich	k_F	342.4	61.6	184.3	52.7	288.2	123.3
	n	0.2835	0.2913	0.3424	0.2837	0.4001	0.2216
	R^2	0.9367	0.8753	0.9831	0.9621	0.9739	0.9432

Comparing adsorption properties of AC and PMCS, two significant phenomenon may require attention: (1) the removal capacities of PMCS enhanced more than 6.0 times for MB, 5.1 times for MO and 4.7 times for CV than those of AC; (2) the adsorption capacities of both MB and CV on AC or PMCS were larger than that of MO. It is well known that the adsorption properties of dyes not only mainly depend on high specific surface area of adsorbents, but also depend on the pore property of adsorbents and size of dye molecular.[37, 38] In this case, the molecule sizes of MB, MO and CV are about ~2 nm, which are smaller than the average pore diameter of PMCS (~12.5 nm), so PMCS with mesostructures can provide much more adsorption sites for dyes.[37, 39] Hence, the differences of adsorption are caused mainly by N_2-BET surface areas and pore-structures of AC (298.4 m^2/g and 0.272 cm^3/g) and PMCS (1023.2 m^2/g and 1.32 cm^3/g). On the other hand, excellent dispersion of PMCS can increase the available adsorption sites, which may be favorable for the aqueous phase adsorption (Fig. S4). The molecules of MB, MO and CV have the similar sizes, while the q_m values of MB and CV are much greater than that of MO, which can be attributed to the more adsorption of cationic dye molecules on the negatively-charged surface of PMCS via some interaction like electrostatic interaction or ion exchange.[38]

The above results revealed that the PMCS exhibited much more favorable adsorption properties and faster adsorption rates than traditional carbon materials. We compared the q_m of PMCS with those of some adsorption materials reported previously (Table S2). It can be seen that PMCS has the highest maximum adsorption capacity of those materials, which suggests that it has great potential application in wastewater treatment engineering in industries due to its excellent adsorption properties.

To further understand the adsorption mechanism of PMCS, the FTIR results were evaluated before and after dye adsorption, as shown in Figs. 7A-7C. The peaks of functional groups -OH (3361 cm^{-1}), C=O (1560 cm^{-1}) and C-O (1056 cm^{-1}) were detected, which further verified the results of XPS analysis. Those functional groups on the surface of PMCS improved its hydrophilicity greatly and also acted as adsorption sites for dye molecules.[38] In the case of MB, a shift in 1197 cm^{-1} (now at 1214 cm^{-1}) was observed, which may correspond to the attachment of MB on the surface of PMCS (Fig. 7A). In the case of MO, two new peaks located at 798 and 895 cm^{-1} were observed after MO adsorption, which belong to in the finger print region. The intensities of peaks at 1548 and 1687 cm^{-1} increased due to -N=N- group attached to the aromatic ring of MO, which indicated that MO had been anchored on the surface of PMCS during the adsorption process (Fig. 7B). As for CV, the sharp peak at 1363 cm^{-1} due to C-N stretching disappeared after CV adsorption (Fig. 7C).

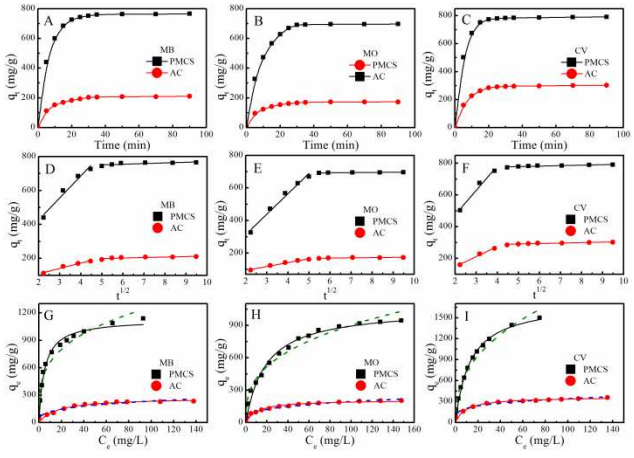

Fig. 6 The adsorption kinetic (A-C), corresponding Weber-Morris model (D-F) and adsorption isotherms (G-I) for MB, MO and CV on PMCS and AC. (Temperature: 25 °C; pH ~6.5)

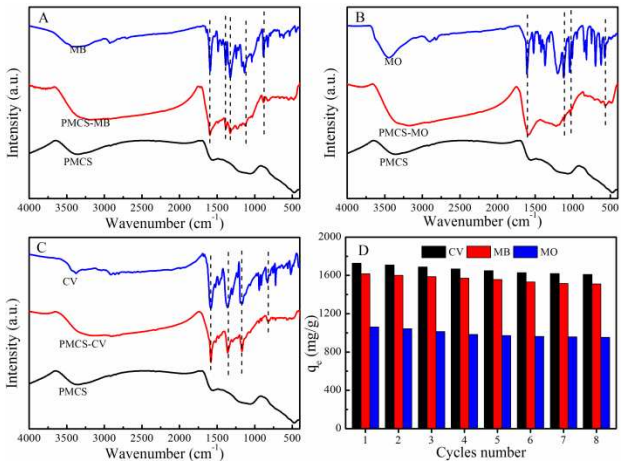

Fig. 7 The FTIR spectra of MB, MO, and CV, and PMCS with or without dyes loading (A-C). (D) The recyclable performance of the PMCS.

In addition, the reusability of the synthesized adsorbent is quite a crucial factor, since better repeated availability can effectively reduce the overall cost of the adsorbent. It can be seen that the PMCS still possesses 98.5%, 97.9% and 97.1% adsorption capacity for MB, CV and MO after eight cycles of reusing, indicating that the PMCS has a good reusability for MB, CV and MO adsorption (Fig. 7D).

As key aspects to appraise one adsorbent material, besides the high sorption capacity, the separation of adsorbent is also extremely important. The magnetic property of PMCS was also investigated, as shown in Fig. 8A. It was calculated that the M_s of the PMCS was ~45.4 emu/g. The photographs for MB, MO, and CV before and after adsorption by the PMCS were shown in Figs. 8C-8D. It can be seen obviously that all dyes were adsorbed completely and the used adsorbents could be separated easily by

an external magnet from the aqueous suspension after adsorption, which was of great importance for real applications. Therefore, the as-prepared PMCS could be applied as a promising adsorbent for the treatment of organic pollutants polluted water in environmental pollution cleanup for its easy separation properties.

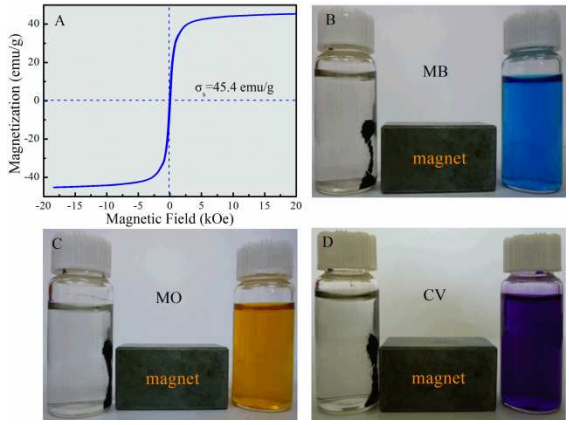

Fig. 8 Room temperature hysteresis loops of PMCS (A), photograph showing the magnetic responsive performance of PMCS after adsorption of MB (B), MO (C) and CV (D).

Conclusions

In summary, novel carbon-stabilized magnetic (Fe/Fe_3C) nanoparticles embedded in porous graphitic carbon sheets were successfully fabricated by a facile and scalable *in-situ* synthetic method with assistance of the graphitic catalyst precursor ($Fe(NO_3)_3$) and template agent ($Al(NO_3)_3$). This magnetic carbon material with porous structure afforded a remarkably enhanced adsorption rate, higher adsorption capacity for MB (1615.9 mg/g), MO (1062.4 mg/g) and CV (1728.3 mg/g), due to its high surface area and large pore volume. Regeneration studies showed the feasibility of adsorbent materials reuse. Meanwhile, the magnetic property allowed PMCS to be separated conveniently and effectively from the solution. Taking into account the simple process, low cost, easy separation, high adsorption capacity and recyclability, this magnetic carbon material can be used as novel, efficient and fast separation adsorbents for the removal of dyes from wastewater in environmental pollution cleanup.

Acknowledgements

The authors acknowledge the financial support from National Natural Science Foundation of China (21225730, 91326202, 21207136 and 21272236), the Ministry of Science and Technology of China (2011CB933700), Hefei Center for Physical Science and Technology (2012FXZY005) and the Priority Academic Program Development of Jiangsu Higher Education Institutions.

Notes and references

[a] *Key Laboratory of Novel Thin Film Solar Cells, Institute of Plasma Physics, Chinese Academy of Sciences, P.O. Box 1126, Hefei, 230031, P. R. China.*
[b] *School of Materials Science and Engineering, Hefei University of Technology, 230031, Hefei, P. R. China*
E-mail: lijx@ipp.ac.cn (J. Li), xkwang@ipp.ac.cn (X. Wang)
Fax: +86-551-65591310; Tel: +86-551-65592788
[c] *School for Radiological and Interdisciplinary Sciences, Soochow University, Suzhou 215123, P.R. China*
Email: xkwang@suda.edu.cn (X. Wang)

† Electronic Supplementary Information (ESI) available: kinetic models (pseudo-first-order and pseudo-second-order), Langmuir and Freundlich isotherm models. See DOI: 10.1039/b000000x/

1. G. Crini, *Bioresource Technol.,* 2006, **97**, 1061-1085.
2. A. Mittal, A. Malviya, D. Kaur, J. Mittal and L. Kurup, *J. Hazard. Mater.,* 2007, **148**, 229-240.
3. S. H. Chen, J. Zhang, C. L. Zhang, Q. Y. Yue, Y. Li and C. Li, *Desalination,* 2010, **252**, 149-156.
4. G. X. Zhao, L. Jiang, Y. D. He, J. X. Li, H. L. Dong, X. K. Wang and W. P. Hu, *Adv. Mater.*, 2011, **23**, 3959-3963.
5. G. X. Zhao, T. Wen, C. L. Chen and X. K. Wang, *RSC Adv.*, 2012, **2**, 9286-9303.
6. Y. X. Zhang, S. C. Xu, Y. Y. Luo, S. S. Pan, H. L. Ding and G. H. Li, *J. Mater. Chem.,* 2011, **21**, 3664-3671.
7. Y. X. Zhang, X. Y. Yu, Z. Jin, Y. Jia, W. H. Xu, T. Luo, B. J. Zhu, J. H. Liu and X. J. Huang, *J. Mater. Chem.,* 2011, **21**, 16550-16557.
8. X. L. Yang, X. Y. Wang, Y. Q. Feng, G. Q. Zhang, T. S. Wang, W. G. Song, C. Y. Shu, L. Jiang and C. R. Wang, *J. Mater. Chem. A,* 2013, **1**, 473-477.
9. X. L. Yu, S. R. Tong, M. F. Ge, J. C. Zuo, C. Y. Cao and W. G. Song, *J. Mater. Chem. A,* 2013, **1**, 959-965.
10. A. Banerjee, R. Gokhale, S. Bhatnagar, J. Jog, M. Bhardwaj, B. Lefez, B. Hannoyer and S. Ogale, *J. Mater. Chem.,* 2012, **22**, 19694-19699.
11. W. Fan, W. Gao, C. Zhang, W. W. Tjiu, J. S. Pan and T. X. Liu, *J. Mater. Chem.,* 2012, **22,** 25108-25115.
12. S. W. Zhang, W. Q. Xu, M. Y. Zeng, J. Li, J. X. Li, J. Z. Xu and X. K. Wang, *J. Mater. Chem. A,* 2013, **1**, 11691-11697.
13. S. W. Zhang, J. X. Li, T. Wen, J. Z. Xu and X. K. Wang, *RSC Adv.,* 2013, **3**, 2754-2764.
14. Y. Jia, X. Y. Yu, T. Luo, M. Y. Zhang, J. H. Liu and X. J. Huang, *Dalton T.,* 2013, **42**, 1921-1928.
15. M. Baikousi, A. B. Bourlinos, A. Douvalis, T. Bakas, D. F. Anagnostopoulos, J. Tucek, K. Safarova, R. Zboril and M. A. Karakassides, *Langmuir,* 2012, **28**, 3918-3930.
16. J. Li, S. W. Zhang, C. L. Chen, G. X. Zhao, X. Yang, J. X. Li and X. K. Wang, *ACS Appl. Mater. Inter.,* 2012, **4**, 4991-5000.
17. J. Hu, D. D. Shao, C. L. Chen, G. D. Sheng, J. X. Li, X. K. Wang and M. Nagatsu, *J. Phys. Chem. B,* 2010, **114**, 6779-6785.
18. Z. X. Wu, W. Li, P. A. Webley and D. Y. Zhao, *Adv. Mater.,* 2012, **24**, 485-491.
19. W. J. Liu, K. Tian, H. Jiang, X. S. Zhahg, H. S. Ding and H. Q. Yu, *Environ. Sci. Technol.,* 2012, **46**, 7849-7856.
20. W. J. Liu, K. Tian, H. Jiang and H. Q. Yu, *Sci. Rep.,* 2013, **3**, 1-7.
21. M. Biswal, K. Bhardwaj, P. K. Singh, P. Singh, P. Yadav, A. Prabhune, C. Rode and S. Ogale, *Rsc Adv.,* 2013, **3**, 2288-2295.
22. Z. H. Wen, S. Q. Ci, F. Zhang, X. L. Feng, S. M. Cui, S. Mao, S. L. Luo, Z. He and J. H. Chen, *Adv. Mater.,* 2012, **24**, 1399-1404.
23. D. H. Liu, G. Yue, L. H. Zhang, W. C. Li, T. Sun and A. H. Lu, *Small,* 2013, DOI: 10.1002/smll.201300276.
24. C. L. Chen, B. Liang, A. Ogino, X. K. Wang and M. Nagatsu, *J. Phys. Chem. C,* 2009, **113**, 7659-7665.
25. K. Y. Yang, W. Xu, Y. Zhang, W. T. Zheng and X. Wang, *Chem. Res. Chinese U,* 2010, **26**, 348-351.
26. W. Li, Z. H. Zhang, B. A. Kong, S. S. Feng, J. X. Wang, L. Z. Wang, J. P. Yang, F. Zhang, P. Y. Wu and D. Y. Zhao, *Angew. Chem. Int. Edit.,* 2013, **52**, 8151-8155.
27. Q. Wang, X. K. Wang, Z. F. Chai and W. P. Hu, *Chem. Soc. Rev.*, 2013, 42, 8821-8834.
28. L. Wang, C. G. Tian, B. L. Wang, R. H. Wang, W. Zhou and H. G. Fu, *Chem. Commun.*, 2008, 5411-5413.
29. T. T. Xie, W. Lv, W. Wei, Z. J. Li, B. H. Li, F. Y. Kang and Q. H. Yang, *Chem. Commun.*, 2013, **49**, 10427-10429.
30. X. Y. Chen, C. Chen, Z. J. Zhang and D. H. Xie, *J. Mater. Chem. A,* 2013, **1**, 10903-10911.
31. Y. Z. Piao, J. Kim, H. B. Na, D. Kim, J. S. Baek, M. K. Ko, J. H. Lee, M. Shokouhimehr and T. Hyeon, *Nat. Mater.,* 2008, **7**, 242-247.

32. S. V. Mohan, N. C. Rao and J. Karthikeyan, *J. Hazard. Mater.,* 2002, **90**, 189-204.
33. C. Gao, X. Y. Yu, T. Luo, Y. Jia, B. Sun, J. H. Liu and X. J. Huang, *J. Mater. Chem. A,* 2013, DOI: 10.1039/C3TA13526H.
34. B. Chen, Z. L. Zhu, J. Ma, Y. L. Qiu and J. H. Chen, *J. Mater. Chem. A,* 2013, **1**, 11355-11367.
35. M. Dogan, H. Abak and M. Alkan, *J. Hazard. Mater.,* 2009, **164**, 172-181.
36. Y. S. Al-Degs, M. I. El-Barghouthi, A. A. Issa, M. A. Khraisheh and G. M. Walker, *Water Res.,* 2006, **40**, 2645-2658.
37. X. Zhuang, Y. Wan, C. M. Feng, Y. Shen and D. Y. Zhao, *Chem. Mater.*, 2009, **21**, 706-716.
38. Y. Dong, H. M. Lin, Q. M. Jin, L. Li, D. Wang, D. Zhou and F. Y. Qu, *J. Mater. Chem. A*, 2013, **1**, 7391-7398.
39. J. Ma, F. Yu, L. Zhou, L. Jin, M. X. Yang, J. S. Luan, Y. H. Tang, H. B. Fan, Z. W. Yuan and J. H. Chen, *ACS Appl. Mater. Inter.,* 2012, **4**, 5749-5760.

TOC

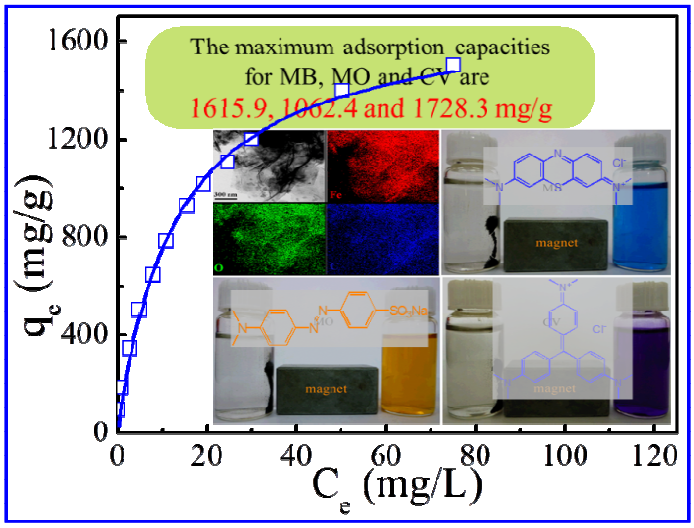

Carbon-stabilized Fe/Fe_3C nanoparticles with excellent adsorption capacity for dyes were fabricated through a facile *in-situ* synthetic strategy.